The Computational Capacity of Memristor Reservoirs

Forrest C. Sheldon[1], Artemy Kolchinsky[2], Francesco Caravelli[1]

[1] *Theoretical Division and Center for Nonlinear Studies,*
Los Alamos National Laboratory, Los Alamos, New Mexico 87545, USA
[2] *Santa Fe Institute, 1399 Hyde Park Road, Santa Fe, NM 87501, USA*

Reservoir computing is a machine learning paradigm in which a high-dimensional dynamical system, or *reservoir*, is used to approximate and perform predictions on time series data. Its simple training procedure allows for very large reservoirs that can provide powerful computational capabilities. The scale, speed and power-usage characteristics of reservoir computing could be enhanced by constructing reservoirs out of electronic circuits, but this requires a precise understanding of how such circuits process and store information. We analyze the feasibility and optimal design of such reservoirs by considering the equations of motion of circuits that include both linear elements (resistors, inductors, and capacitors) and nonlinear memory elements (called memristors). This complements previous studies, which have examined such systems through simulation and experiment. We provide analytic results regarding the fundamental feasibility of such reservoirs, and give a systematic characterization of their computational properties, examining the types of input-output relationships that may be approximated. This allows us to design reservoirs with optimal properties in terms of their ability to reconstruct a certain signal (or functions thereof). In particular, by introducing measures of the total linear and nonlinear computational capacities of the reservoir, we are able to design electronic circuits whose total computation capacity scales linearly with the system size. Comparison with conventional echo state reservoirs show that these electronic reservoirs can match or exceed their performance in a form that may be directly implemented in hardware.

I. INTRODUCTION

Reservoir computing (RC) [1–3] is a recently-proposed paradigm for performing computations on time series data, which combines a high-dimensional driven dynamical system (or *reservoir*) with a simple learning algorithm. RC has proven to be a powerful tool in a wide variety of signal processing tasks, including forecasting [1], pattern generation and classification [4], adaptive filtering and prediction of chaotic systems [5]. Recent extensions of reservoir computing to spatio-temporal chaotic systems [6] have proven surprisingly effective, and are under active investigation.

Central to the success of reservoir computation is the use of large, recurrently connected reservoirs to generate nonlinear transformations and store memories of the driving signal. This has generated interest in developing nanoscale electronic reservoirs with large number of elements [7], incorporating both linear components (such as resistors, inductors, and capacitors) and nonlinear components such as *memristors*. Memristors, or "resistors with memory", are nanoscale devices that allow the input of memory degrees of freedom in the electrical response of certain materials. The currents flowing through these devices cause a rearrangement of ions, leading to a persistent (but also reversible) change in resistance. Memristors offer the possibility of harnessing both nonlinear behavior and non-trivial memory in electronic circuits. For this reason, specialized circuits composed of large numbers of such devices promise a new generation of computational hardware operating orders of magnitude faster, and at far lower power, than traditional digital circuitry [8–13].

The success of reservoir computing requires a precise understanding of how the reservoir processes and stores information. It is known how to optimize performance and tune parameters in conventional reservoirs such as echo state networks (ESNs) [3]. However, electronic reservoirs based on memristors have some attention lately, with most work being based on simulations or experiments [14–16], and some analytical work in [17, 18]. In this paper we provide a systematic and analytical study of the computational capacity of memristor reservoirs with different architectures.

In this paper, we fill this gap by first characterizing the types of input-output relationships can be computed by various electrical circuits with memory. We then utilize this characterization to guarantee three specific computational properties of electronic reservoirs: feasibility, tunability, and scalability. In order to be *feasible* as a reservoir, a driven dynamical system must satisfy a set of properties which guarantee that its state encodes an informative function of the driving signal; we establish feasibility for models of linear/LRC (inductor-resistor-capacitor) and memristor reservoirs. A reservoir's computational properties must also be *tunable* to the computational problem at hand. We characterize the input-output relationships natural to electronic reservoirs, in the process showing how memristors may be viewed as a source of nonlinear computations. We then demonstrate how to combine linear and nonlinear elements to achieve a specific computational task (that of approximating a 2nd order filter). Lastly, the capacity of the reservoir to perform useful computations should *scale* as the size (i.e., dimensionality) of the reservoir is increased. In particular, one of the main motivation for electronic reservoirs is the potential to achieve very large reservoir sizes, but such increases are useless if they do not lead to improved computational capacities of the reservoir. Optimally, the number of linearly independent inputs that the reservoir can reconstruct should scale linearly with the reservoir size — i.e., to borrow a term from statistical physics, they should they should be *extensive* in reservoir size. For both LRC and memristor reservoirs, we consider measures of linear and nonlinear computational capacity, and show that they can be made to scale extensively.

In the next section we make these notions more precise. We provide a formal development of reservoir computing, electronic reservoirs and memristors, as well as definitions of the measures of computational capacity we will utilize. We then turn to the feasibility, tunability and scalability of LRC and memristor-based reservoirs. Finally, we compare our results to more conventional ESN reservoirs [1], showing that electronic reservoirs are capable of matching or exceeding the performance of a standard ESN reservoir implementations.

BACKGROUND

Reservoir Computing

Reservoir computing is a machine learning technique for approximating a mapping between two sequences or functions. In what follows, we present a brief review of reservoir computing in continuous time, assuming scalar-valued input and output functions. The translation to discrete time and vector-valued inputs/outputs is straightforward.

Formally, a reservoir combines a multivariate dynamical system with a simple learning algorithm. At time t, the state of the dynamical system, which we indicate as $\vec{x}(t)$, is driven by an input $u(t)$ and obeys the differential equation

$$\dot{\vec{x}}(t) = F(\vec{x}(t), \vec{u}(t)). \tag{1}$$

As a result of these dynamics, the state of the reservoir encodes information both about its previous history and (possibly nonlinear) transformations of the input. As an important example, a linear reservoir is governed by the equation

$$\dot{\vec{x}}(t) = A\vec{x}(t) + \vec{u}(t). \tag{2}$$

In the following, we will choose $\vec{u}(t) = \vec{v}u(t)$, where $\vec{v}$ is a vector which defines how the input signal $u(t)$ enters into each neuron (or in general memory element). In order for a dynamical system to be considered *feasible* as a reservoir, its state must approach a function of the input trajectory. At a high level, we can state this requirement in terms of two conditions:

- *Fading Memory*: If the system were to be started from two different initial conditions $\vec{x}_0, \neq \vec{x}_0'$ and driven with the same input trajectory u, the system's trajectories should eventually converge to the same state, $\vec{x}(t), \vec{x}'(t) \to \vec{x}[u](t)$ as $t \to \infty$. The statement above implies that the system has a finite temporal memory.

- *State Separation*: Different input sequences should drive the system into different trajectories, i.e., if the same initial condition were to be driven with two different input trajectories $u \neq u'$, the state of the system is reflected in the difference at long times. Mathematically, here we use the local-time notion, e.g. that $\|\vec{x}[u](t) - \vec{x}[u'](t)\| > 0 \ \forall t > 0$.

The first condition is analogous to requiring that the state of the reservoir becomes a function of the input trajectory, while the second requires that the this function carries information about the input trajectory. More precisely this allows us to regard the reservoir as implementing a *filter* of the input trajectory (e.g. it modifies the projection on a certain Hilbert space). In this sense, reservoir computers can be thought of as approximating filters, in much the same that neural networks may be considered as approximating functions [19, 20].

In addition to the input trajectory u, we are also provided with an output trajectory z. We assume this output trajectory is generated by some (typically complicated and nonlinear) function of the input trajectory u, and so sometimes write it as $z[u]$. The goal of reservoir computing is to learn to approximate the input-output mapping $u \mapsto z[u]$ with an estimate $\hat{z}[u]$, which is defined as a linear combination of the reservoir's variables, $\hat{z}[u](t) = \vec{w}^T \vec{x}[u](t)$. This is displayed schematically in figure 1, with variable names referring to the relevant quantities in electronic circuits. To the reservoir trajectories $\vec{x}$ we typically append the a constant signal, $\vec{x}'(t) := [\vec{x}(t), \vec{1}(t)]$ as is common practice in RC.

While the reservoir is typically a large and recurrently connected dynamical system, the interesting feature of RC is that only the output layer, given by the coefficients $\vec{w}$, is trained. Training is performed in the following manner. First, the reservoir is "initialized" by driving with the input signal on an interval $[-T', 0]$, until the fading memory property ensures that its state is independent of the initial condition at $t = -T'$. The reservoir is then driven for an additional interval $[0, T]$. The coefficients $\vec{w}$ are learned via linear regression, by minimizing the mean squared error (MSE) between a reconstruction $\hat{z}(t) = \vec{w}^T \vec{x}'(t)$ and the provided output trajectory $z(t)$ over the time interval $[0, T]$,

$$\text{MSE}_T[z, \vec{w}] = \frac{1}{T} \int_0^T dt \, (z(t) - \vec{w}^T \vec{x}'(t))^2. \tag{3}$$

This optimization problem $\hat{\vec{w}} = \text{argmin}_{\vec{w}} \text{MSE}_T[z, \vec{w}]$ has a closed form solution $\hat{\vec{w}} = (\vec{x}'^T \vec{x}')^{-1} \vec{x}' z^T$, with the resulting approximation $\hat{z}(t) = \hat{\vec{w}}^T \vec{x}'(t)$ being the projection of $z(t)$ onto the span of the reservoir trajectories. Regularization via ridge regression is also commonly employed in practice, which modifies the objective to $\text{MSE}_T[z, \vec{w}] + k\|\vec{w}\|^2$.

The Computational Capacity of Continuous Time Reservoirs

A framework for defining and assessing the computational capacity of reservoirs was developed by Dambre *et al.* [21] in the context of discrete time reservoirs. Here we deal with its extension to continuous time reservoirs [22].

The goal of RC is to approximate the *function* $u \mapsto z[u]$, rather than simply the value of this function $z(t)$ on the training interval $t \in [0, T]$. In order to distinguish the trajectories, one has to define a notion of distance between reservoir trajectories $\vec{x}[u]$ and the output function $z[u]$, which we do by employing an appropriate Hilbert space on the set of trajectories. Within such Hilbert space, Dambre *et al.* introduce the subset of trajectories called "fading memory Hilbert space", which contains functions that possess the fading memory property
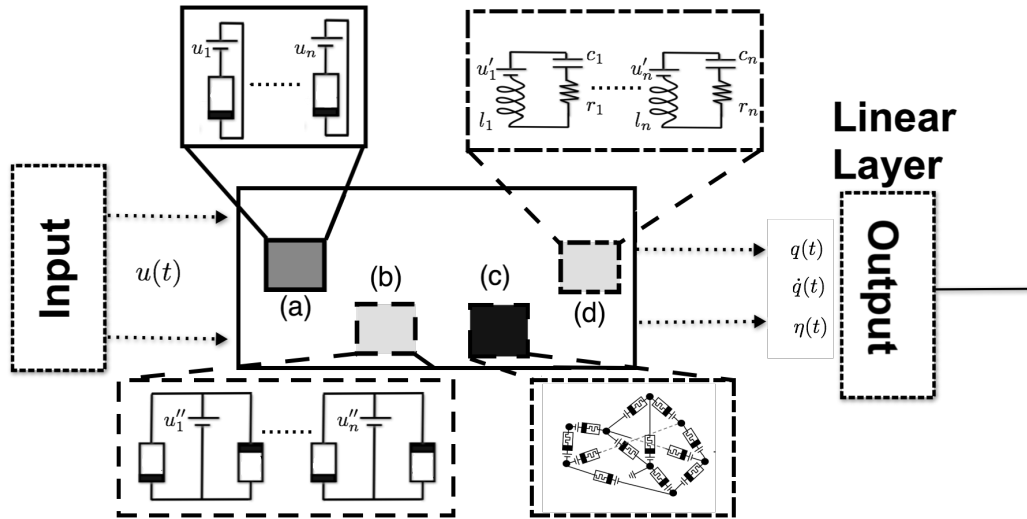
Figure 1. Scheme of an electronic reservoir. The input $u(t)$ for an electronic reservoir is a voltage, internal states $\vec{x}(t)$ are given by dynamical resistive states $R(t)$ (or internal memory states $m(t)$ which define the resistance for a memristor), voltages $u(t)$ or charge $q(t)$. The reservoir we propose has various modules with a different role, and memristors are introduced for nonlinear learning tasks. Specifically, we propose modules which include LRC circuits (top right), polar memristor circuits (top left), apolar memristive circuits (bottom left) and memristive networks (bottom right). As we will see, simple apolar memristive circuits have similar computational property of memristive networks.

discussed above (i.e., they depend only on the recent history of the input).

The inner product on the space of trajectories is constructed by defining a measure over inputs u as well as an associated inner product as $\langle z, z' \rangle = E_u \big[\int_0^\infty z[u](t) z'[u](t) dt \big]$, where E_u indicates expectation over the measure. For a reservoir that satisfies our notion of feasibility, the state trajectories will be elements of this Hilbert space. In practice, ergodicity may be leveraged to compute inner products in terms of time averages of reservoir trajectories, rather than over the measure over u. Thus, by introducing a random input signal and averaging over sufficiently long times we can regard our results as measuring properties of the *reservoir* rather than the particular time interval used for training. We also inherit the linear structure of the Hilbert space with notions or orthogonality, dimension and distance.

Measures of Capacity

We are interested in the estimator that minimizes the MSE of eqn. (3) for some target output z. Following Dambre *et al.* [21], we define the memory capacity of the dynamical system to approximate z as

$$C_T[z] = 1 - \frac{\min_{\vec{w}} \text{MSE}_T[z, \vec{w}]}{\langle z^2 \rangle_T}, \qquad (4)$$

where $\langle f \rangle_T = \frac{1}{T} \int_0^T dt\, f(t)$. The capacity is bounded $0 \le C_T[z] \le 1$. In what follows, in addition to the memory capacity $C_T[z]$, we will also reference the normalized mean-squared error of the estimate, $\text{nMSE}_T[z] = 1 - C_T[z]$.

An immediate consequence of the above definitions is that, when evaluated on a complete set of orthogonal functions and

in the long time limit, the sum of capacities will tend towards the number of linearly independent trajectories in the reservoir, i.e., the size of the span of the reservoir trajectories. Since an approximation can only be accurate when $z[u]$ is close to the span of the reservoir, the number of linearly independent trajectories in the reservoir puts a strong constraint on the possible effectiveness of the reservoir. As shown numerically in [21], there is in fact a tradeoff between the linear memory capacity of a reservoir, and the amount of nonlinear reconstruction ability[23]. For this reason, it is possible to tune the system towards one or the other feature.

By evaluating $C_T[z]$ for different choices of z, one can quantify the capacity of the reservoir to perform different kinds of computations. For example, when z is a linear function of the input u, $C_T[z]$ will quantify capacity to perform linear computations, and when z is a nonlinear function of the input u, $C_T[z]$ will quantify capacity to perform nonlinear computations. Given this, we note two points that will guide our development of electronic reservoirs: (1) A reservoir must be tunable, by which we mean that it can be designed so as to achieve high $C_T[z]$ for different desired choices of z. For echo state networks, various rules of thumb for tuning their performance have been developed; we will present analogous methods for obtaining high values of specific $C_T[z]$ in electronic networks; (2) Based on these capacities, we can build a measure of total memory capacity (see τ_ϵ below) which should scale with the size of the reservoir. The success of RC draws from the ability to use very large reservoirs. If electronic reservoirs are to be useful, increasing the size of the reservoir must improve its performance on the type of capacities we chose in (1). Optimal scaling is extensive in the system size. In what follows we develop measures of capacity for different kinds of z that we will be interested in.

The memory capacity $C_T[z]$ generalizes several common measures of reservoir performance. For example, the previously-proposed "memory function" $m(\tau)$ [2, 22, 24] captures the reservoir's capacity to reconstruct linear functions of the input at time lag τ. By defining the time-lagged input trajectory $u_\tau(t) = u(t - \tau)$, we can write in terms of the memory capacity as $m(\tau) = C_T[u_\tau]$. This offers a natural generalization to nonlinear functions $m_n(\tau_1, \ldots, \tau_n) = C_T[u_{\tau_1} \cdot u_{\tau_2} \ldots u_{\tau_n}]$ which measures the reservoir's capacity to produce products of the input function taken at previous times $\tau_1, \ldots \tau_n$.

We introduce a measure of the total linear memory capacity of the network,

$$\tau_\epsilon = \int_0^\infty d\tau \, \Theta(m(\tau) > 1 - \epsilon), \tag{5}$$

where Θ is the Heaviside step function, which we refer to as the *linear memory capacity* of the dynamical system. This quantity captures the time delay at which the history of the input is reconstructed with an error less than ϵ. This definition can be generalized to quantify the total *nonlinear memory capacity* as

$$\tau_\epsilon^{(n)} = \int_0^\infty \cdots \int_0^\infty d\tau_1 \cdots d\tau_n \, \Theta(m_n(\tau_1, \ldots, \tau_n) > 1 - \epsilon). \tag{6}$$

In [24], a discrete time linear reservoir is presented with a $\tau_{0.5}$-memory length that scales extensively with the system size. This is translated to continuous time in [22] using a different measure of total capacity. In this work we present an electronic implementation of the linear reservoirs discussed in those papers, alongside an implementation which includes nonlinear components. We then generalize this approach by designing an electronic reservoir which displays extensive scaling in its quadratic-memory capacity $\tau_\epsilon^{(2)}$.

Circuit Elements and Structure

We consider circuits composed of traditional linear elements including inductors (L), capacitors (C), and resistors (R), active elements (voltage or current sources), as well as passive memory elements known as memristors (Mem) (see below). In all cases, the electronic reservoir will accept a vector input through a set of voltage sources $\vec{s}$. We can convert the scalar input $u(t)$ to a time dependent voltage vector through a set of input weights $\vec{s} = \vec{v}u(t)$.

The linear reservoirs we consider will be composed of sets of LRC subcircuits as shown in figure 1 (d) in which each LRC circuit, indexed by n has component values l_n, r_n, c_n and is driven by a voltage generator $s_n = u(t)$ (taking $\vec{v} = \vec{1}$). Each circuit possesses two degrees of freedom $q_n(t), \dot{q}_n(t)$ corresponding to the charge across and current entering the capacitor, which follow equations of motion,

$$\begin{bmatrix} \dot{q}_n(t) \\ \ddot{q}_n(t) \end{bmatrix} = \begin{bmatrix} 0 & I \\ -\frac{1}{l_n c_n} & -\frac{r_n}{l_n} \end{bmatrix} \begin{bmatrix} q_n(t) \\ \dot{q}_n(t) \end{bmatrix} + \begin{bmatrix} 0 \\ \frac{s_n(t)}{l_n} \end{bmatrix}. \tag{7}$$

The output trajectories of an LRC are the trajectories of the internal degrees of freedom, $\vec{x} = [\vec{q}(t), \dot{\vec{q}}(t)]$ (the vector notation covers the indexing over n). The dimension of an LRC reservoir of N subcircuits is thus $2N$.

In addition to the linear electronic reservoirs described above, we consider reservoirs of nonlinear electronic components called memristors. Memristors are passive 2-terminal devices characterized by the current-input response relationship,

$$V(t) = R(\eta)I(t), \tag{8}$$

$$\dot{\eta}(t) = f(\eta(t), I(t)), \tag{9}$$

where $V(t)$ is the voltage drop across the memristor, $I(t)$ is current, $\eta(t)$ is the internal state of the memristor, and $R(\eta(t))$ is the state-dependent resistance. It can be seen that the resistance can depend on the past history of the current. Importantly, memristors are inherently nonlinear elements. We will consider several circuit structures as shown in figure 1, including single memristor circuits (a), paired memristor circuits (b) and memristor networks (c). As in the case of linear networks, the input to the circuits is through a set of voltage generators $\vec{s}(t) = \vec{v}u(t)$ where $\vec{v}$ is a vector of weights with units of voltage.

The internal states of a memristor circuit closely mimic the behavior of a neural network. We constrain ourselves to the linear current model similar to the one proposed in [9], along with a decay term [25],

$$R(\eta) = R_{\text{off}}(1 - \eta) + R_{\text{on}}\eta, \tag{10}$$

$$R(\eta) = R_{\text{off}}(1 - \chi\eta) \quad \left(\chi := \frac{R_{\text{off}} - R_{\text{on}}}{R_{\text{off}}}\right), \tag{11}$$

$$\dot{\eta} = -\alpha\eta + \frac{1}{\beta}I(t). \tag{12}$$

Here the constant $\alpha = 1/t^*$ is an inverse time scale while β is an activation current per unit of time, which moderates the strength of the input signal. Thus, $I(t) = V(t)/R(\eta(t))$. We see that for $\alpha = 0$, $\eta(t)$ is proportional to the total charge accumulated in the conductor. We limit η to the interval $[0, 1]$, so the resistance $R(\eta)$ varies between two limiting values $[R_{\text{on}}, R_{\text{off}}]$.

The various circuit structures in figure 1 may be cast in a universal form by introducing the cycle space projector Ω_A [25] which projects onto current configurations that satisfy Kirchhoff's current law. The projector Ω_A can be simply computed from the circuit graph $\mathcal{G}$. in which nodes of the graph $n \in \mathcal{G}$ represent electrical junctures between the edges that contain electrical elements. For a circuit in which the edges contain a voltage generator in series to a memristor, as in figure 1 (c), the equation of motion is given by [25]

$$\dot{\vec{\eta}}(t) = -\alpha\vec{\eta}(t) + \frac{1}{\beta}(I - \chi\Omega_A H(t))^{-1}\Omega_A\vec{s} \tag{13}$$

where we have used the convention $H(t) = \text{diag}\,\vec{\eta}(t)$. Interactions between memristors thus occur through the inverse of $I - \chi\Omega_A H(t)$ and are mediated both by χ and the Kirchhoff laws imposed by Ω_A. A memristor circuit generates reservoir trajectories $vecx = [\vec{\eta}(t)]$ which are used to train the output.

RESULTS

Linear Electronic Reservoirs

In this section we illustrate the notions of capacity and scaling introduced above in the more familiar realm of linear circuits. In the following, we show that electronic reservoirs with extensive memory capacity may be constructed from LRC circuit components and that these devices may be understood as constructing the Fourier representations of linear kernels. Moreover, in the Materials and Methods, we prove the following result.

Feasibility of LRC circuits. *Reservoirs of separate LRC circuits (as described in the following) satisfy the fading memory and state separability properties.*

This justifies our use of these systems as reservoirs and the application of the capacity measures above. For the linear reservoir in eqn. (2), the long time limit solution is

$$\vec{x}(t) = \int_0^\infty d\tau e^{A\tau} \vec{v} u(t - \tau), \qquad (14)$$

from which we see that linear reservoirs may be used to approximate linear functions of the input signal, and that their properties will depend on the eigenvalues of A. A natural measure in which to demonstrate extensive scaling is thus the memory capacity τ_n. In [22, 24] it was noted that an extensive memory capacity was obtained for reservoirs with eigenvalues lying on a vertical line in the negative half plane, *i.e.,* eigenvalues of the form $\lambda_{n,\pm} = -\gamma \pm in\Delta\omega$ for $n \in \{0 \dots N\}$. The resulting trajectories of the system can be implementing a truncated Fourier transform with cut-off $\omega_c = N\Delta\omega$ and base frequency $\Delta\omega$. The exponential window, $e^{-\gamma\tau}$ indicates that this will be successful for an interval $0 \leq \tau \leq 1/\gamma$ and that the base frequency $\Delta\omega$ should be on the same order as γ.

A series LRC circuit expressed as a linear system has eigenvalues $\lambda_\pm = -\frac{r}{2l} \pm i\sqrt{\frac{1}{lc} - \frac{r^2}{4l^2}} = -\gamma \pm i\omega$ and a corresponding pair of trajectories $q_n(t)$, $\dot{q}_n(t)$ corresponding to the charge and current entering the capacitor (see Materials and Methods). As a consequence *any eigenvalue spectrum in the negative half-plane and symmetric in the upper and lower half planes can be achieved by a collection of LRC circuits with a particular choice of the component values l_n, r_n, c_n,* as in Fig. 1 (d). Given a γ and $\Delta\omega$, we choose $l_n = 1$, $r_n = 2\gamma$ for all n and

$$c_n = \frac{1}{n^2 \Delta\omega^2 + \gamma^2} \qquad (15)$$

in which case we have that the resulting LRC circuits have eigenvalues $\lambda_{n,\pm} = -\gamma \pm in\Delta\omega$.

Recalling a particular memory, $z_\tau(t) = u(t - \tau)$ is thus equivalent to constructing an approximate representation of the delta function $\delta(t - \tau)$. After fitting, the learned weights w_{q_n}, $w_{\dot{q}_n}$ and w_c may be used to construct the 'kernel' of the

reservoir. Specifically, we can write the predicted output as

$$\hat{z}(t) = \sum_{n=1}^N \left(w_{q_n} q_n(t) + w_{\dot{q}_n} \dot{q}_n(t) \right) + w_c \qquad (16)$$

$$= \int_0^\infty d\tau \, K(\tau) u(t - \tau) + w_c. \qquad (17)$$

where K indicates the kernel function,

$$K(\tau) = e^{-\gamma\tau} \sum_{n=1}^N \frac{1}{l_n n \Delta\omega} \Big[w_{q_n} \sin(n\Delta\omega\tau) +$$
$$w_{\dot{q}_n} \big(n\Delta\omega \cos(n\Delta\omega\tau) - \gamma \sin(n\Delta\omega\tau) \big) \Big], \quad (18)$$

which gives an explicit representation of the network's approximation to $\delta(t - \tau)$. In Figure 2, we display the memory function, kernel and reconstruction for an LRC circuit reservoir with $\gamma = 0.12$, $\Delta\omega = 0.7\gamma$ and 71 subcircuits (motifs) corresponding to an cutoff frequency of $N\Delta\omega = 6Hz$. We can see that the memory function can reconstruct the signal with a fairly long delay.

To construct an LRC network of N circuits, we identify a maximum frequency $\omega_{\max}$ associated with our signal and define $\Delta\omega = \omega_{\max}/N$ as the lowest frequency and resolution. This lowest frequency defines a timescale $t^* \sim 1/\Delta\omega$ over which a periodic signal could be represented by the Fourier series. We then choose $\gamma = \sqrt{2}\Delta\omega$ to suppress the signal for times longer than t^*. From this we expect, if $\omega_{\max}$ is chosen sufficiently large to accurately represent the signal, that the system's linear memory capacity τ_ϵ will scale as N. This is confirmed in figure 3, where we show the linear memory capacity τ_ϵ for $\epsilon = 0.1$ across a range of reservoir sizes. As expected, reservoirs of this type show an extensive linear memory capacity. Note that the precise value of ϵ is unimportant since, as shown in figure 2, the memory function for these networks maintains a value near 1 before falling sharply.

MEMRISTOR RESERVOIRS

We now turn to establishing analogous results for memristor reservoirs. To begin, in the Materials and Methods we prove the following results:

Feasibility of Memristor Networks. *Reservoirs of networked memristors satisfy the fading memory and state separability properties for sufficiently small input signal.*

In memristor networks, fading memory is a consequence of the decay term $-\alpha x$ in the equations of motion, eqn. (12), which represents the volatility of the conductive state. Some degree of volatility is thus an asset to memristors employed in RC.

Having established feasibility we now turn to the specific functional forms of the memristor trajectories. Generalizing the representation of linear systems in eqn. (14), functions in the fading memory Hilbert space have a representation as a
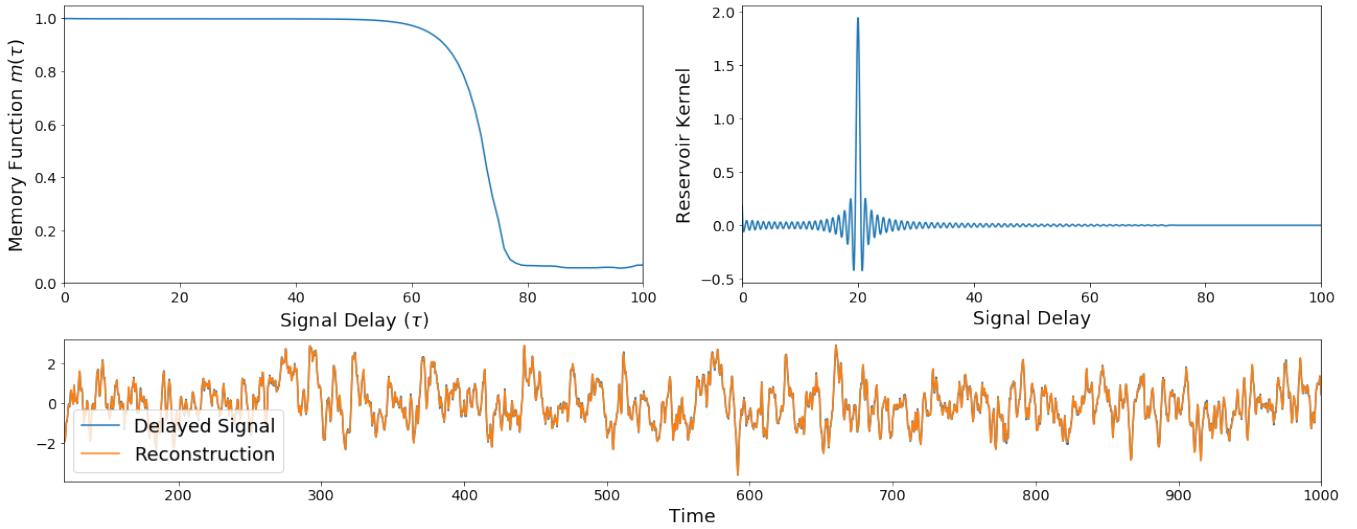
Figure 2. The (linear) memory function $m(\tau)$ (upper left), kernel (upper right) and reconstruction (lower) for an LRC circuit reservoir with $\gamma = 0.12$, $\Delta\omega = 0.7\gamma$ and 71 elements corresponding to an cutoff frequency of $N\Delta\omega = 6Hz$. The memory function maintains a value above 0.99 up to a delay of 55.5. The kernel is calculated from the analytical solution of the network and fitted weights. This figure shows that the LRC reservoir takes advantage of its Fourier modes to construct a sinc approximation to the δ function. The bottom panel displays the resulting reconstruction at $\tau = 20$. For this delay, the reconstruction obeys $m(\tau) = 0.9983$.
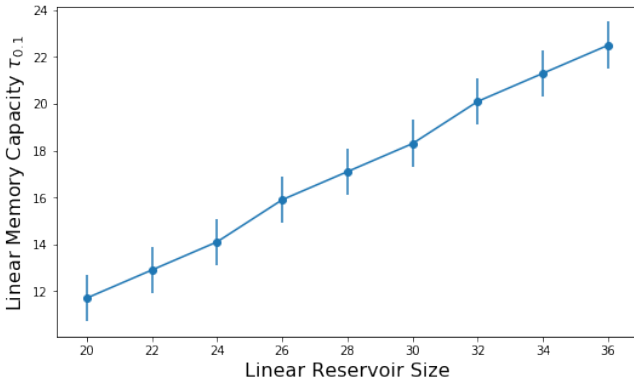

Figure 3. The extensive scaling of the linear memory capacity $\tau_{0.1}$ with the number of trajectories generated in an LRC reservoir. The construction of the reservoirs, detailed in the main text and Materials and Methods, corresponds to $\omega_{\max} = 4$ Hz. Errors are shown as vertical bars.

Wiener/Volterra series [26],

$$z[u](t) = \int_0^\infty d\tau_1\, h_1(\tau_1)u(t - \tau_1)$$
$$+ \int_0^\infty d\tau_1 d\tau_2\, h_2(\tau_1, \tau_2)u(t - \tau_1)u(t - \tau_2) + \cdots \tag{19}$$

which decomposes the function into linear and progressively higher order nonlinear components governed by kernel functions $h_n(\tau_1, \ldots \tau_n)$.

The trajectory of a single memristor governed by eqn. (12)

has the Volterra series expansion

$$\eta(t) = \frac{1}{\beta} \int_0^\infty d\tau_1 e^{-\alpha\tau_1} u(t - \tau_1) +$$
$$\frac{\chi}{\beta^2} \int_0^\infty d\tau_1 \int_{\tau_1}^\infty d\tau_2\, e^{-\alpha\tau_2} u(t - \tau_1)u(t - \tau_2) + O(\chi^2), \tag{20}$$

(see Materials and Methods), where we have neglected boundary effects and where higher order kernels of the input are suppressed by higher powers of χ. We immediately note that the kernel functions tend to be exponentially decaying at a rate determined by α, consistent with the fading memory property and the fact that memristor trajectories depend on arbitrarily high powers of the driving signal $u(t)$. In this sense, memristors may be considered as a source of nonlinearity in electronic reservoirs.

Given our notion of tunability, we wish to demonstrate how to design memristor reservoirs for particular computational problems, i.e. a particular choice of z. As a generalization of the linear case, we consider the approximation of an arbitrary 2nd order filter with support on the previous time interval $[0, T^*]$. More specifically, we wish to approximate a function of the input with the form,

$$z[u](t) = \int_0^{T^*} d\tau_1\, F_1(\tau_1)u(t - \tau_1) +$$
$$\int_0^{T^*} d\tau_1 \int_0^{T^*} d\tau_2\, F_2(\tau_1, \tau_2)u(t - \tau_1)u(t - \tau_2).$$

Approximating this function with memristors requires isolating terms related to the second order contribution to the trajectory. In this interest we note that considering a reservoir of two

memristors $\eta_+(t)$ and $\eta_-(t)$ each driven by $u(t)$ and $-u(t)$ respectively, allows us to construct their sum (away from the boundaries and up to terms of order $O(\chi^2)$) as

$$\eta_\pm(t) \approx \frac{2\chi}{\beta^2} \int_0^\infty d\tau_1 \int_{\tau_1}^\infty d\tau_2\, e^{-\alpha\tau_2} u(t - \tau_1) u(t - \tau_2)$$

where $\eta_\pm(t) = \eta_+(t) + \eta_-(t)$, which cancels all odd terms in $u(t)$.

Due to the exponential decay with time of terms in the Wiener/Volterra series, we expect the system to only be able to construct nonlinear functions of the input over a relatively short time delay. A decreased value of α will integrate a longer window of the previous history into the current state, but will also lead to lower capacity due to interference from previous memories. As in the case of the LRC circuit, it is essential to vary the parameters of the circuits to generate linearly independent trajectories. This may be accomplished by varying α and β (the timescales of decay/excitation for memristors), by varying the amplitude of the driving, or by introducing disorder into the structure of the circuit Ω_A. Here we focus on what we view as the most practical option, which is varying the amplitude of the driving signal. In networks, memristors are driven with a proximal voltage generator that varies in amplitude from $+C$ to $-C$ in equally spaced increments, where C is a constant that may be tuned.

In Figure 4 we provide comparisons between reservoirs composed of LRC, Single Memristors, Paired Memristors and Memristor networks. While on the one hand the LRC circuit is able to reconstruct only linear transformations of the input, memristive networks have only a limited advantage over paired disconnected memristor motifs.

While memristor reservoirs give us the ability to calculate quadratic functions of the input with high accuracy for short times, the quadratic memory capacity $\tau_\epsilon^{(2)}$ does not scale extensively as the size of the reservoir is increased. This can be seen from the fact that the memristor network reservoirs, which is 28 times bigger than the "paired memristors" reservoir, has a similar quadratic memory capacity. In the next section we consider hybrid reservoirs of memristor and LRC components which do demonstrate this scaling.

Hybrid Deep Reservoirs

The properties of LRC and memristor reservoirs may be combined to improve the scaling of the nonlinear capacities of interest. The reservoir structure we will examine uses the trajectories of a "surface layer" reservoir $\vec{x}_s(t)$ where voltage generators are driven by the input, $\vec{s}_s = \vec{v}u(t)$, to drive another "deep layer" reservoir $\vec{x}_d$ [27]. The deep layer voltage generators are driven by the surface layer trajectories as $\vec{s}_d = C\vec{x}_s$ where C is a matrix of coupling coefficients whose structure is discussed below. As LRC and memristor components are kept in separate layers, these deep reservoirs inherit the feasibility properties of their sub-components. The training procedure uses all trajectories $\vec{x} = [\vec{x}_s, \vec{x}_d]$ in the regression.

As seen in Figure 4, the ability of memristors to calculate quadratic functions of the input occurs only over a brief time.

The results above would suggest that using a surface layer memristor network to drive a deep layer LRC reservoir would yield a substantial improvement of the interval over which the reservoir could yield a successful quadratic reconstruction. In figure 5, the top panel shows the result of using a pair of memristors configured as in the section above, to drive an LRC reservoir. Each memristor trajectory $\vec{x}_s = [\eta_+(t), \eta_-(t)]$ is used as a source signal for a small LRC reservoir of 10 circuits with $\gamma = 0.4$, $\Delta\omega = 0.4$ corresponding to a cutoff frequency of $4\ Hz$ to produce additional trajectories $\vec{x}_d = [\vec{q}_+(t), \dot{\vec{q}}_+(t), \vec{q}_+(t), \dot{\vec{q}}_+(t)]$. As such, C is a 40×2 matrix in which the first 20 rows were $[1, 0]$ and the subsequent 20 $[0, 1]$ The resulting reservoir trajectories are used to evaluate the quadratic memory function m_2 with the results showing a substantial increase in the systems computational capacity for 'equal-time' quadratic reconstructions (defined via $m_2(\tau, \tau)$). As the deep LRC reservoir is used to recall the equal-time products computed by the memristor reservoir, we expect that measures of their total quadratic capacity $\tau_\epsilon^{(2)}$ will also scale extensively. However increasing the reservoir size will not improve the reconstruction of unequal-time products.

We may similarly consider the effect of using a surface layer LRC reservoir to drive a deep layer memristor reservoir. In this case, products of the Fourier modes stored in the LRC network state will be computed by the memristor network, offering something akin to a 2-dimensional Fourier transform in τ_1 and τ_2. We thus suspect the resulting network will display an improved unequal-time quadratic memory function. To accomplish this, we have implemented a the same 10 circuit LRC reservoir as described above driven with the input signal. The resulting 20 trajectories are coupled to a set of memristor pairs such that the sum and difference of every pair of the 20 LRC trajectories are used to drive an independent pair of memristors (the structure of the coupling matrix C is given in the supplemental information). The resulting $2 \times 20 \times 19 + 20 = 780$ trajectories are used to train the reservoir. In the lower panel of figure 5 we have implemented this to calculate the quadratic memory function. We observe a substantial improvement in the reservoir's ability to construct unequal-time products of the input signal although this requires an increase in the size of the reservoir. Such an increase is expected, as the number of unequal-time products with $\tau_1, \tau_2 < T$ scales quadratically in the maximum delay T. In figure 6 we show the scaling of $\tau_{0.1}^{(2)}$ with the size of the reservoir. The total quadratic capacity indeed scales linearly with the size of the reservoir indicating that arbitrary unequal-time products may be reconstructed by a sufficiently large reservoir. We emphasize that it is the nonlinear memory capacity $\tau_\epsilon^{(2)}$ that can scale extensively with the system size; increasing the maximum delay T under which we can reconstruct products of the input will require that the reservoir size scale as T^2.

A natural further architecture to consider would be to use memristor reservoirs as both surface and deep layers, as has been considered in works based on the simulation of these devices. Given the discussion above, we expect the primary benefit of this architecture is to enhance higher order nonlinear capacities which is precisely what we observe in simulation.
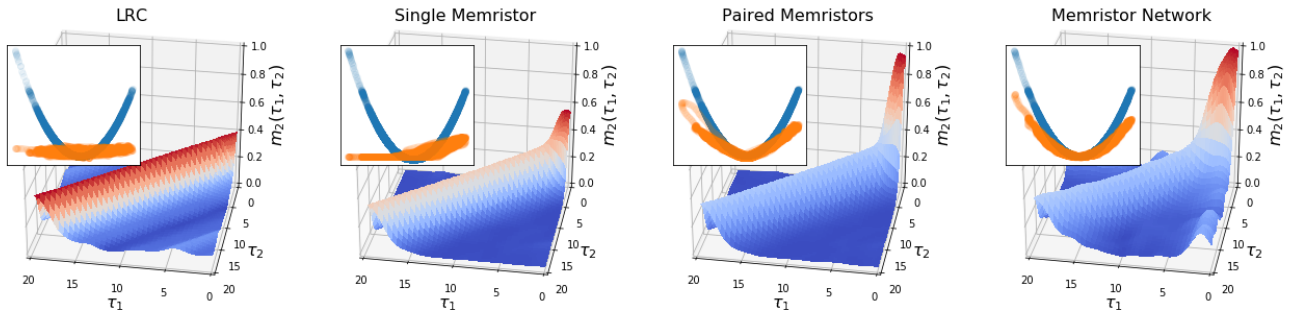
Figure 4. The quadratic memory function $m_2(\tau_2, \tau_2)$ for LRC circuits (left), a single (middle left) and opposed pair (middle right) of memristors and a triangular lattice of memristors (right). This measures the reservoirs ability to approximate the function $z(t) = u(t - \tau_1)u(t - \tau_2)$. We define $\tau^* := \mathrm{argmax}_\tau m_2(\tau, \tau)$, which corresponds to the optimal delay for an equal time reconstruction; the insets show the corresponding reconstruction $\hat{z}$ (orange) and target output $z(t) = [u(t - \tau^*)]^2$ (blue) as a function of the input signal $u(t - \tau^*)$. As expected, the LRC circuit, as in Fig. 1 (d) is only capable of generating linear approximations of the output. A single memristor reservoir, as in Fig. 1 (a) is unable to isolate its quadratic component and misses negative parts of the reconstruction due to boundary effects (middle left inset). The addition of another memristor with opposite bias, as in Fig. 1 (b), significantly increases the ability to reconstruct z. The memristor network, Fig. 1 (c), shows an enhanced ability to reconstruct z and clear nonlinearity (right inset). The nonlinear memory function value of $m_2(\tau^*, \tau^*)$ for each network was 0.390 (LRC), 0.558 (single memristor), 0.960 (paired memristors), and 0.995 (memristor network).

However, as this is outside the scope of the computational task we set out to achieve, we do not include results from such networks here.

Comparison with Echo State Networks

To assess the performance of these electronic reservoirs against standard reservoirs, we construct a fitting task in which we must approximate a known function of the input signal. We construct a member of the fading memory Hilbert space as

$$z[u](t) = \int_0^{10} d\tau\, K_1(\tau)u(t - \tau) +$$
$$\int_0^{10} d\tau_1 \int_0^{10} d\tau_2 K_2(\tau_1, \tau_2)u(t - \tau_1)u(t - \tau_2)$$
$$(21)$$
$$K_1(\tau) = e^{-0.5\tau}\cos(2\tau) \qquad (22)$$
$$K_2(\tau_1, \tau_2) = -e^{-0.3\tau}\cos\big(2(\tau_1 - \tau_2)\big) \qquad (23)$$

the accurate approximation of which requires a mixture of memory and nonlinearity.

To approximate this, we apply an implementation of continuous time Echo State Network (ESN) for comparison. An ESN is a dynamical reservoir in which the internal states evolve according to

$$\dot{\vec{x}} = -\alpha\vec{x}(t) + \tanh(M\vec{x}(t) + \vec{u}(t)), \qquad (24)$$

where α here is a leakage similar to the one of the memristor devices we consider, while $\tanh(\cdot)$ applies to every neuron; M is a matrix that in order to satisfy the fading property must have maximum eigenvalue less than one; $\vec{u}$ scales the magnitude of the input $u(t)$ as it drives each neuron.

We compare the results of a tuned ESN to a "naive" memristor network analogous to those employed in previous literature,

Table I. Comparison of reservoir performance on the quadratic filtering task described in the main text.

Reservoir	dim($\vec{x}$)	nMSE	Gen. nMSE
'Naive' Memristor Network	800	0.1(8)	(2).
ESN	780	0.02(0))	0.03(6)
LRC→Memristor	780	0.01(4)	0.01(8)

and a hybrid LRC to memristor reservoir. As far as possible, each reservoir was configured to produce the same number of trajectories.

The "naive" memristor network is a 17×17 triangular lattice with 800 edges each containing a memristor ($\alpha = 3$, $\beta = 1$, $\chi = 0.8$) and voltage generator. The driving input was varied on the interval $[-1, -0.1] \cup [0.1, 1]$ (see Materials and Methods for further information). The LRC→Memristor reservoir was configured identically to that presented above included a total of 780 trajectories. Finally the ESN consisting of 780 elements was run and tuned following the recommendations in [3] (see Materials and Methods).

We report both the training error, calculated on an input output pair on $[100, 4000]$ and a measure of generalization error, using the trained weights to reconstruct the output on $[4000, 5000]$ (see Materials and Methods). The hybrid LRC→Memristor reservoir demonstrates a 10-fold improvement over the 'naive' memristor network and performs on par with the ESN implementation in training as well as a 2-fold improvement in generalization error. Suitably crafted analog reservoirs are thus capable of matching and even surpassing the performance of standard reservoirs.
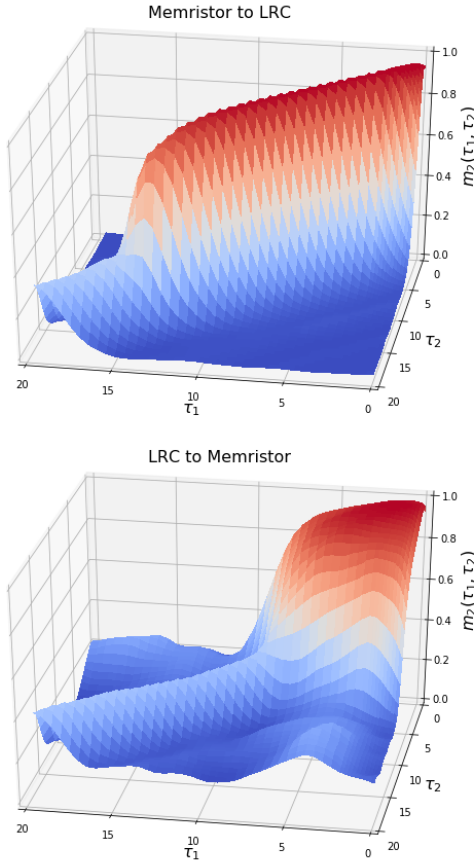
Figure 5. The quadratic memory function $m_2(\tau_1, \tau_2)$ for hybrid memristor-LRC reservoirs. The top panel shows the result of using a driven pair of memristors to drive an LRC reservoir. The LRC reservoir stores memory of the nonlinear computation in the memristor network, leading to large equal time quadratic capacities. In the lower panel, the result of using an LRC reservoir to drive a set of memristor pairs is shown. The memristor pairs compute products of the Fourier modes generated in the LRC network, approximately implementing a 2-dimensional Fourier transform, though this is effective only for short times.

DISCUSSION

Despite wide interest in the possibility of utilizing electrical circuits with memory as the basis for hardware reservoirs, an understanding of how these systems process and store information has been lacking. While for echo state networks, the balance between memory and nonlinearity is controlled primarily by the spectral radius of the coupling matrix, no similar conditions have been explored for electrical networks.

In this work we have shown that linear electronic reservoirs of LRC circuits can be constructed with optimal memory properties, having an eigenvalue spectrum known to correspond to an extensive memory (e.g. that scales linearly with the number of components). We have shown that this may be interpreted as performing a Fourier transform of the driving signal in hardware and that the eigenvalue spectrum required can be
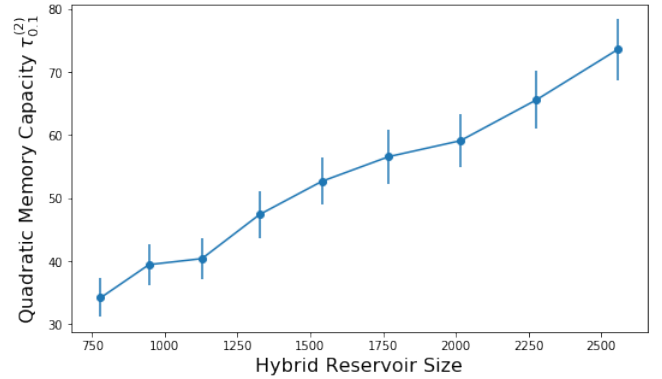

Figure 6. The scaling of the quadratic memory capacity with reservoir size in the hybrid LRC to Memristor reservoir. LRC reservoirs ranging from 10 to 18 subcircuits were used to drive a memristor reservoir as described in the main text, resulting in reservoirs ranging from 946 to 2556 internal degrees of freedom. The quadratic memory capacity $\tau_{0.1}^{(2)}$ (and errorbars) were estimated from a finite size scaling analysis as detailed in the Materials and Methods.

designed appropriately for a given problem.

In memristor reservoirs we have shown that while the system contains contributions from terms of very high order, these are moderated in strength by powers of χ. It is essential that the reservoir be able to isolate desired terms to make use of them in the training process; we have shown that using paired memristors of opposite polarity gives a substantial increase in the reservoir's ability to isolate their quadratic kernels.

Combining LRC and memristor networks into deep reservoirs allows the utilization of the memory capabilities of LRC reservoirs and the nonlinear capacities of memristor reservoirs in order to obtain specific computational capacities. Utilizing an LRC network as a deep layer allows nonlinear computations performed in the surface memristor network to be stored for long times. Similarly, using an LRC reservoir as the surface layer driving a deep layer memristor network will calculate products of Fourier modes and give enhanced unequal time quadratic capacities. Most importantly, this leads to a total quadratic capacity which scales linearly with the system size such that arbitrary products of the input can be constructed by a sufficiently large reservoir.

This analysis can have substantial impacts on performance, as we show in our comparison to ESN reservoirs. The hybrid reservoirs we present give a 10-fold improvement over the naive memristor network implementation, and perform on par with the ESN implementation. Properly constructed electronic reservoirs should thus be capable of matching the performance of standard reservoirs but also open the use of larger reservoirs and faster computation times.

The approach we take to the analysis of the computational capacities of memristor and LRC reservoirs may be generalized to higher order kernels of the network and other nonlinear elements. In this sense we attempt to present a general approach to the understanding of physical reservoirs in analogy to the methods available to tune ESNs by trading between memory storage and nonlinearity.

The ability to design effective reservoirs for low-dimensional tasks implies their effectiveness on high dimensional tasks such as fluid dynamics and spatiotemporal chaos through parallelization [6]. Designing flexible co-processors consisting of networks of low-dimensional reservoirs, similar to those presented here, will require a careful understanding of their computation properties and how to modify them to the task at hand. This work fills a gap in this understanding, allowing for tuneable electronic reservoirs to be implemented in hardware.

MATERIALS AND METHODS

Input signals

In order to construct an ensemble of input signals with a specified autocorrelation length we consider a delta-correlated noise process $\xi(t)$ such that

$$\langle\xi(t)\rangle = 0, \quad \langle\xi(t)\xi(t')\rangle = D\delta(t - t'). \tag{25}$$

From this we construct an input signal by smoothing $\xi(t)$ with a timescale $1/a$,

$$u(t) = \int_{-\infty}^{\infty} d\tau\, e^{-a|t-\tau|}\xi(\tau) \tag{26}$$

in which case $\langle u(t)\rangle = 0$ and $\langle u(t)u(t+\tau)\rangle = D(\tau+\frac{1}{a})e^{-a\tau}$. We thus obtain random input signal with unit autocorrelation time and unit variance by choosing $D = 1$, $a = 1$. Further details about the construction of the input signal are given in the supplemental information.

Reservoir Training

Once a set of trajectories $\vec{x}(t)$ were generated on the interval $[0, 5000]$ the portion of the trajectory on $[0, 100]$ was removed as a transient. The remaining trajectories had a constant vector appended and training was then performed using scikit-learn's `Ridge` regression method. In all cases the ridge regression parameter was set to $k = 0.0001$ such that the regularization of the weights was minimal.

LRC simulations

For Figure 2, the LRC network was constructed with $\gamma = 0.12$, $\Delta\omega = 0.7\gamma$, and 71 LRC circuit elements corresponding to a cutoff frequency of $N\Delta\omega = 6Hz$.

Achieving an estimate of the exact representation of the kernel in eqn. (18) required a close correspondence between simulations and the exact formula over many autocorrelation times of a rapidly oscillating system. As most integration schemes would lead to a small buildup of phase differences over these periods, we used the exact representation of the system trajectory to simulate the reservoir. The long-time limit solution of the reservoir is given by

$$\begin{bmatrix} q(t) \\ \dot{q}(t) \end{bmatrix} = \frac{1}{l(\lambda_+ - \lambda_-)} \begin{bmatrix} 1 & 1 \\ \lambda_+ & \lambda_- \end{bmatrix} \begin{bmatrix} \int_0^\infty d\tau\, e^{\lambda_+\tau}u(t-\tau) \\ -\int_0^\infty d\tau\, e^{\lambda_-\tau}u(t-\tau) \end{bmatrix} \tag{27}$$

where $\lambda_\pm = -\frac{r}{2l} \pm i\sqrt{\frac{1}{lc} - \frac{r^2}{4l^2}} = -\gamma \pm i\omega$. Simply integrating this is computationally inconvenient as it requires the evaluation of the integral over the full timecourse for every timestep. To avoid we first consider the top integral in eqn. (51). Transforming the integral and using that $u(t) = 0$ for

$t < 0$, we have

$$f_+(t) = \int_0^\infty d\tau e^{\lambda_+\tau}u(t-\tau)$$
$$= \int_0^t d\tau e^{\lambda_+(t-\tau)}u(\tau). \tag{28}$$

The second integral may be recovered from this as $f_-(t) = \Re[f_+(t)] - i\Im[f_+(t)]$. The function $f_+(t)$ then obeys the recursion relation for a timestep Δt,

$$f_+(t + \Delta t) = e^{\lambda_+ t}\left(f_+(t) + \int_0^{\Delta t} d\tau\, e^{-\lambda_= \tau}u(t+\tau)\right). \tag{29}$$

which allows for an exact calculation of the trajectory with a single integral and integration over the interval $[0, 5000]$ with a timestep of $\Delta t = 0.05$. After training, the resulting weights were used to estimate the kernel in figure 2 from eqn. (18). Integration was performed using scipy's quadrature package.

Quadratic Capacity Figure

The LRC network was the same as that described above. Memristors used had $\alpha = 3$, $\beta = 3$, $\chi = 0.8$. Memristor integrations were done using forward Euler method with a stepsize $\Delta t = 0.02$ on eqn. (13). For single or paired memristors, $\Omega_A = I$, $\alpha = 3$, $\beta = 3$ and $\chi = 0.8$. Paired memristors use one element subject to $+u(t)$ and the other subject to $-u(t)$. In all memristor simulations hard boundaries are imposed on the integration to maintain $w \in [0, 1]$. The memristor network consisted of a 5×5 triangular lattice with 56 memristor-voltage generator edges. Each voltage generator was weighted with weights distributed evenly on the set $[-1, -0.1] \cup [0.1, 1]$.

Hybrid Network Figure

The top panel of figure 5 shows a reservoir composed of two memristors driven with opposite polarity, used to drive an LRC network of 10 elements. The memristors were configured and simulated as described in the above section. The trajectory of each memristor, $x_\pm(t)$ was used to drive an independent LRC reservoir with $\gamma = 0.4$, $\Delta\omega = 0.4$, and $N = 10$ corresponding to a cutoff frequency of 4 Hz. Each LRC reservoir generated 20 trajectories of the form $q_{n\pm}, \dot{q}_{n\pm}$ for $n = 1\ldots10$. Memristor trajectories were calculated using forward Euler with a timestep of $\Delta t = 0.02$ and eqn. (13).

For the LRC to Memristor reservoir, first the trajectories of an LRC network of 10 circuits as described above were calculated using the driving signal on the interval $[0, 5000]$. From the LRC trajectories $\vec{x}_s = [\vec{q}, \dot{\vec{q}}]$ we define a coupling matrix to the deep memristor layer, $\vec{s}_d = C\vec{x}_s$ such that every sum and difference of trajectories in $\vec{x}_s$ is used to drive an independent memristor pair. As such, for every $i, j \in \{1\cdots10\}$ there are

$k_1 \ldots k_4$ such that

$$s_{d,k_1} = x_{s,i} + x_{s,j}, \ s_{d,k_2} = -s_{d,k_1}$$
$$s_{d,k_3} = x_{s,i} - x_{s,j}, \ s_{d,k_4} = -s_{d,k_3}$$

Each of these voltage generators drives a memristor with $\alpha = 3, \beta = 3, \chi = 0.8$. The reservoir thus contains $2 * 20 * 19$ memristors and generates 20 LRC trajectories giving 780 independent trajectories. As this reservoir contains an LRC network at its surface layer, it also has excellent linear computation capacities, maintaining a computational capacity greater than 0.99 to a delay of $\tau = 10$.

Linear and Quadratic Memory Scaling

To estimate the memory capacity of LRC networks with system size, networks were generated with N = 10,... 18 subcircuits. For each reservoir, the cutoff frequency was chosen as 4 Hz, the frequency resolution as $\Delta\omega = 4/N$, and $\gamma = \Delta\omega$. The resulting reservoirs were driven with an input sequence on $[0, 5000]$. Training was then performed to reconstruct the delayed input $u(t - \tau)$. To evaluate τ_ϵ, a bijective search was performed to evaluate the delay at which the memory function $m(\tau) = C_T[u(t - \tau)]$ fell below the threshold $1 - \epsilon$, terminating with a tolerance of 1. Finite size scaling analysis was found to be unnecessary as the calculated capacities did not vary with the length of the training interval. Error estimates are from the termination criteria of the bijective search.

To estimate the quadratic memory capacity $\tau_\epsilon^{(2)}$, the trajectories of the LRC reservoirs above were used to drive deep memristor networks as described in the hybrid reservoir section of the main text. To evaluate $\tau_\epsilon^{(2)}$, we wish to find the area over which $m_2(\tau_1, \tau_2) > 1 - \epsilon$. First a bijective search was run along the diagonal to find the delay τ^* at which the quadratic memory function $m(\tau, \tau)$ fell below $1 - \epsilon$. Then the function was integrated numerically over $\tau_1 \in [0, 2\tau^*]$ $\tau_2 \in [0, 2\tau^*]$ with subdivisions of 0.5. This provides an uncertainty in the numerical integration on the order of $e_{int} = 2 * 0.5 * *2 * np.sqrt(\tau_\epsilon^{(2)})$.

The quadratic capacities $\tau_\epsilon^{(2)}$ show clear tendencies towards overestimation for smaller training intervals and larger reservoir sizes. To combat this, we employed a finite size scaling analysis to estimate the capacity $\tau_\epsilon^{(2)}$ in the limit of an infinite training interval. A figure demonstrating this analysis is included in the supplemental information. We also note that linear and nonlinear memory functions were found to decrease rapidly outside of a region of support. As a consequence, capacities $\tau_\epsilon^{(n)}$ depend only weakly on ϵ. However, for small values of ϵ fluctuations play a larger role and make capacities difficult to estimate numerically. We found $\epsilon = 0.1$ struck a reasonable balance between high capacities and low fluctuations on estimates. Errors from the fit are estimated through the elements of the covariance matrix as $e_{fit} = \sqrt{cov_{ii}}$ where i is the index of the constant constant fitting parameter. The total error estimate is given as $e_{tot} = np.sqrt{e_{int}^2 + e_{fit}^2}$.

Comparison to Echo State Networks

For all tested reservoirs, trajectories were generated on $[0, 5000]$ with training performed on $[100, 4000]$ giving a training error estimate of the nMSE. To assess the generalization error, the weights from the previous training were used to reconstruct the output on $[4000, 5000]$ and a generalization nMSE was calculated as,

$$\text{Gen. nMSE} := \frac{\langle (z(t) - \hat{z}(t)) \rangle_T}{\langle z^2(t) \rangle_T} \tag{30}$$

where the average $\langle \cdot \rangle_T$ is performed over the generalization window $[4000, 5000]$. Note that, unlike the nMSE, this quantity is not constrained to fall within $[0, 1]$.

For the 'naive' memristor network implementation, parameters were taken as $\alpha = 3$, $\beta = 1$, $\chi = 0.8$ with inputs weighted on the set $[-1, -0.1] \cup [0.1, 1]$. The network graph was chosen as a 17×17 triangular lattice with 800 edges. Input weights were generated as 400 evenly spaced weights on $[0.1, 1]$, another 400 on $[-1, -0.1]$.

The hybrid LRC→Memristor reservoir was implemented identically as above.

The ESN reservoir obeyed the differential equation

$$\dot{\vec{x}} = -\vec{x} + \tanh\left(\Omega\vec{x} + \vec{r}_b + \vec{r}_i u(t)\right) \tag{31}$$

where Ω is a generic matrix of interaction weights between neurons, $\vec{r}_b$ is a bias vector and $\vec{r}_i$ is a vector of input weights. In our case, Ω was chosen to be sparse with a constant fanout of 10, and each weight was initially chosen randomly as ± 1. After generating this matrix it was scaled to obtain a maximum spectral radius of $r = 0.95$ which was found to give best performance on the fitting task. The bias and input weights were selected uniformly on $[-1, 1]$ and were each independently scaled. Both had a range of acceptable performance centered around 0.2 for the bias weight scaling and 0.1 for the input weight scaling with nMSE ranging from 0.020 to 0.023. Integration was performed with forward Euler on the interval $[0, 5000]$ with a timestep of $\Delta t = 0.05$.

SUPPLEMENTAL INFORMATION

Input Signal

The notions of computational capacity were originally developed in the context of discrete time reservoirs. Central to the introduction of the fading memory Hilbert space is the definition of an inner product between functions in terms of an expectation over an ensemble of input signals. Specifically, for functions $z[u]$ and $z'[u]$ that depend only on the previous h timesteps, the inner product between these is defined as the expectation over the ensemble of previous histories, $\langle z, z' \rangle = E_{U^h}[zz']$ where U^h is the space of previous histories where each timestep is i.i.d. sampled from a distribution $p(u)$. The resulting input signals are uncorrelated $\langle u(t - \tau_1)u(t - \tau_2) \rangle = \sigma^2 \delta_{\tau_1, \tau_2}$. The computational capacity
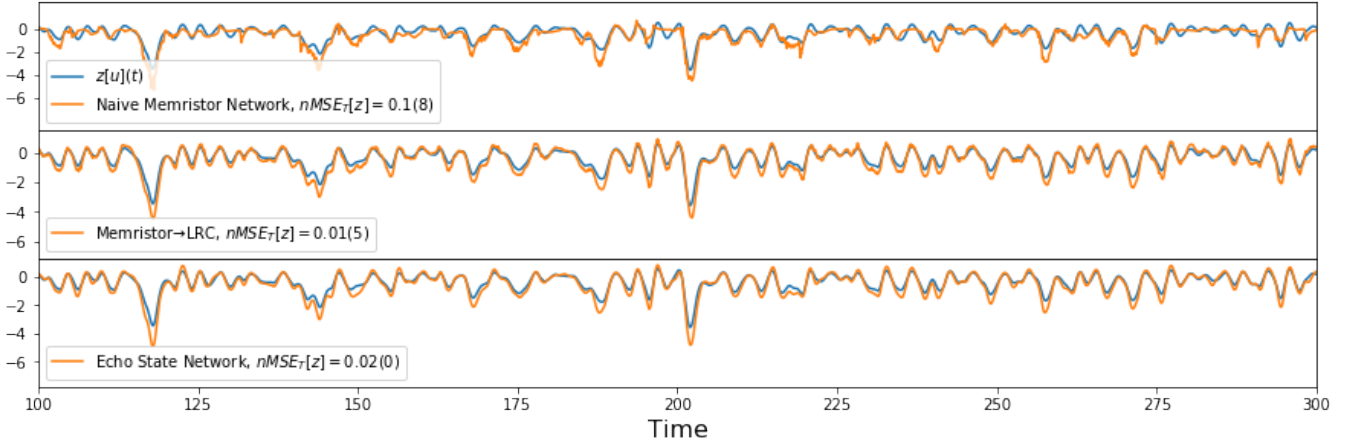
Figure 7. A comparison between memristor, hybrid and echo state network reservoirs on the fitting task described in eqn. (21). In the top panel, we show the results of a 'naive' implementation of a memristor reservoir consisting of a triangular lattice of 800 memristors. In the middle panel we show the results from the hybrid LRC→Memristor reservoir with a total of 780 trajectories. In the bottom panel, we show an echo state network implementation contains 780 elements with parameters tuned to the fitting task. In the legends note that the hybrid networks have a 12-fold improvement over the memristor network alone, perform on par with the ESN implementation.

for reconstructing linear functions of the input thus measure the ability to recall the exact state of the input signal at some previous time.

In continuous time we must cope with the introduction of the timescale of our reservoir. A dynamical system will have some characteristic timescale over which it can vary and will generally display an autocorrelation function that is decreasing with the time difference on that same timescale, *e.g.* for a system with timescale t^*, $\langle x(t)x(t-\tau)\rangle = f(\tau/t^*)$. In formulating an input signal we have two options for how to proceed.

One would be to drive the system with a noise process $\xi(t)$ which maintains the uncorrelated feature of the driving process from discrete time, $\langle \xi(t)\xi(t-\tau)\rangle = 2D\delta(\tau)$. The reservoir would no longer be able to construct the rapid variations of the noise process, but we could assess how well the system computed various filters of this noise, for example $z(t) = \int_0^\infty d\tau e^{-\alpha\tau}\xi(t-\tau)$. In this setting however, the connection to previous work is indirect and requires choosing particular timescales in which to perform memory reconstructions.

Alternatively, following [22] we can produce a signal that varies on the appropriate timescale by filtering a noise process and utilize this as the driving signal of our reservoir. We choose to proceed along this route as it most resembles the tasks towards which reservoir computing is applied. As a signal, we elected to use gaussian white noise smoothed by a double-exponential window with a timescale $1/a$

$$u(t) = \int_{-\infty}^{\infty} d\tau\, e^{-a|t-\tau|}\xi(\tau) \tag{32}$$

where

$$\langle \xi(t)\rangle = 0, \quad \langle \xi(t)\xi(t')\rangle = D\delta(t-t'). \tag{33}$$

Applying these relationships we have $\langle u(t)\rangle = 0$ and $\langle u(t)u(t+\tau)\rangle = D(\tau + \frac{1}{a})e^{-a\tau}$. We thus obtain random

input signal with unit autocorrelation time and unit variance by choosing $D = 1$, $a = 1$. Note that over short times the characteristic timescale is $\frac{1}{2a}$.

In figure 8 we show a sample input signal trajectory (top panel), the resulting autocorrelation function (middle panel) and the resulting power spectral density (bottom panel). The autocorrelation function panel contains both a sample autocorrelation function, calculated from a single trajectory of the input, and the analytical autocorrelation function above.

Feasibility Properties of LRC reservoirs

As the reservoir is composed of independent LRC circuits, it suffices to consider a single circuit. An LRC circuit with component values l, r, and c can be cast as the linear system,

$$\dot{\vec{x}} = \begin{bmatrix} 0 & 1 \\ -\frac{1}{lc} & -\frac{r}{l} \end{bmatrix} \vec{x} + \begin{bmatrix} 0 \\ \frac{s(t)}{l} \end{bmatrix} = A\vec{x} + \vec{u}. \tag{34}$$

where A has eigenvalues $\lambda_\pm = -\frac{r}{2l} \pm i\sqrt{\frac{1}{lc} - \frac{r^2}{4l^2}} = -\gamma \pm i\omega$ with negative real part.

Fading Memory

We first establish that reservoirs composed of LRC motifs satisfy the fading-memory property, namely that two identical reservoirs begun in states x_0 and x_0' and subject to the same driving signal $\vec{u}(t)$ will converge to the same state, $\lim_{t\to\infty} x(t) - x'(t) = 0$.

For $\Delta\vec{x} = \vec{x} - \vec{x}'$

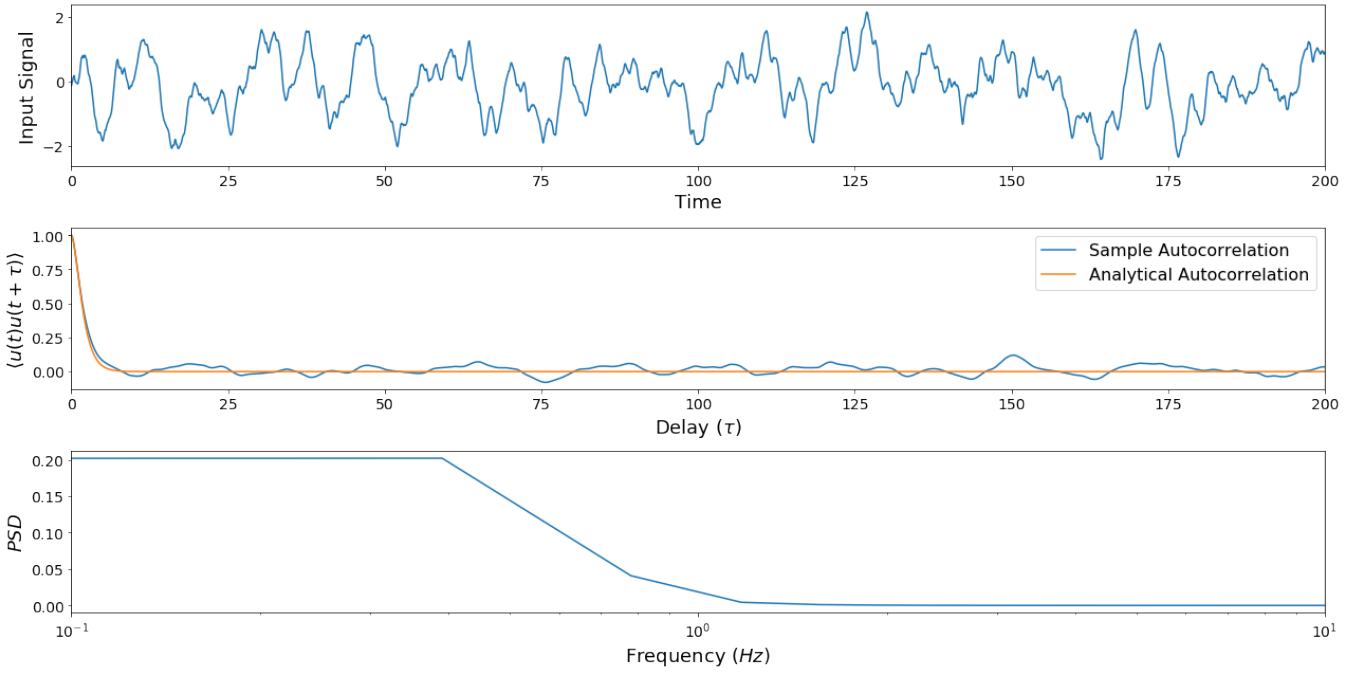$$\frac{d}{dt}\Delta\vec{x} = A\Delta\vec{x} \tag{35}$$

Figure 8. A sample input signal trajectory (top panel), corresponding autocorrelation function (middle panel) and power spectral density (PSD) (bottom panel). The input signal was constructed by smoothing Gaussian white noise with a double exponential window with time constant $1/a$. The resulting autocorrelation function displays a long time exponential decrease as $e^{-a\tau}$. In simulations we set $a = 1$. The power spectral density of the resulting signal contains significant contributions only from frequencies below 1.

with solution

$$\Delta x(t) = e^{At}\Delta \vec{x}(0). \tag{36}$$

As the eigenvalues of A have negative real part $-\frac{r}{2l}$, the difference between the trajectories will converge to 0 as $e^{-\frac{r}{2l}t}$.

State Separability

The equation of motion above for two reservoirs subject to driving signals $\vec{u}(t)$ and $\vec{u}'(t)$ with $\Delta \vec{u}(t) = \vec{u}(t) - \vec{u}'(t)$ leads to the equation of motion,

$$\frac{d}{dt}\Delta \vec{x} = A\Delta \vec{x} + \Delta \vec{u}(t). \tag{37}$$

Two reservoirs begun in the same state $\Delta \vec{x}(0) = 0$ will thus be initially diverging at a rate proportional to the difference between their respective driving signals. In the long time limit, the difference between trajectories can be solved explicitly as,

$$\Delta \vec{x}(t) = \int_0^\infty d\tau e^{A\tau}\Delta \vec{u}(t - \tau). \tag{38}$$

The difference between the two reservoirs is thus identical to a reservoir driven with the difference of the inputs.

Feasibility Properties of Memristor Reservoirs

We consider a reservoir composed of memristors, and where the single memristor, idealized as a switch between two resistance values $R_{\text{off}} > R_{\text{on}}$, is described by a parameter $0 \le \eta_i \le 1$

$$\frac{d}{dt}\eta_i(t) = -\alpha\eta_i(t) + \frac{I_i(t)}{\beta} \tag{39}$$

where $I_i(t)$ is the current in the device, with a resistance of the device is given by $R(\eta) = R_{\text{off}}\big(1 - \eta(t)\big) + R_{\text{on}}\eta(t)$; α and β are phenomenological parameters setting the decay and excitation of the device. It is convenient to write the equation in terms of the parameter $\chi = \frac{R_{\text{off}} - R_{\text{on}}}{R_{\text{off}}}$, which is naturally less than one if $R_{\text{off}} > R_{\text{on}}$.

A memristor network is a model for a general circuit composed of memristors and with voltage generators in series to the memristors, given by the following vectorial and nonlinear differential equation [25]:

$$\frac{d\vec{\eta}}{dt} = -\alpha\vec{\eta}(t) + \frac{1}{\beta}(I - \chi\Omega_A H(t))^{-1}\vec{S} \tag{40}$$

while we do not go into the detail of the derivation of the equation, we point out that Ω_A is a projector operator on the cycle space of the circuit, e.g. $\Omega^2 = \Omega$, while $M_{ij} = \delta_{ij}m_i(t)$.

The input to the network can be voltages in series to the memristors, injected at the nodes, or current sources in parallel or injected at the nodes. For all these cases, we have

respectively [28]

$$\vec{S} = \begin{cases} \Omega_A \vec{s} & \text{Voltage sources in series} \\ A(A^T A)^{-1} \vec{s}_{ext} & \text{Voltage sources at nodes} \\ \Omega_B \vec{j} & \text{Current sources in parallel} \\ B^T(BB^T)^{-1} \vec{j}_{ext} & \text{Current sources at nodes.} \end{cases}$$

While in the paper we focus on the voltages in series, and thus $\vec{S} = \Omega_A \vec{s}$, the proof below is general. Given the equation above, we now prove some of the key properties for the dynamical system to be feasible as a Reservoir, assuming that we read-out either the voltage or the current in the device.

Fading Memory

Let us now discuss the problem of using memristors as a reservoir. First, we consider discrete dynamics in which we use an Euler integration scheme to study the convergence.

First, let us define the echo state property. Let X be the set of internal states of the reservoir. Then

(Echo State Property). A network $F : X \times U \to X$ (with the compactness condition) has the echo state property with respect to U: if for any left infinite input sequence $u^{-\infty} \in U^{-\infty}$ and any two state vector sequences $x^{-\infty}, y^{-\infty} \in X^{-\infty}$ compatible with $u^{-\infty}$, it holds that $x_0 = y_0$.

One of the two properties which are desirable is the fact that different internal initial state with identical external driving converges to the same asymptotic state. This is also called the echo state, or contracting, or fading, property.

Specifically, consider two network states $\vec{\eta}$ and $\vec{\eta}'$. Following the proof by Jaeger for ESNs, we have that for the case of memristor dynamics, we have

$$||\vec{y}_{k+1}||_2 = ||\vec{\eta}_{k+1} - \vec{\eta}'_{k+1}||_2$$
$$= ||(1 - \alpha')\vec{y}_k - \frac{1}{\beta}\left(g(H) - g(H')\right)\vec{S}||_2$$
$$\leq (1 - \alpha')||\vec{y}_k \frac{1}{\beta'} - \left(g(H) - g(H')\right)\vec{S}||_2$$
$$\leq (1 - \alpha')||\vec{y}_k||_2 + \frac{1}{\beta}||g(H) - g(H')||_{\sup}||\vec{S}||_2$$

where $g(H) = (I - \chi\Omega_A f(H))^{-1}$, and $\alpha' = dt \cdot \alpha$ and $\beta' = \frac{\beta}{dt}$. For "linear" memristors, $f(H) = H$. Here we consider for the proof a discretized version of the dynamics (using an Euler scheme), but show that the final result is independent from the step size of the discretization.

We would like to prove that

$$||\vec{y}_{k+1}||_2 \leq C||\vec{y}_k||_2 \qquad (41)$$

with $C < 1$. Let us thus focus on $||g(H) - g(H')||_{\sup}$. We now use the second resolvent identity for the matrix $A = \chi\Omega_A f(H)$ and $z = 1$, and write the following bound

$$||(I - \chi\Omega_A f(H))^{-1} - (I - \chi\Omega_A f(H'))^{-1}||$$
$$\leq \chi||(I - \chi\Omega_A f(H))^{-1}||$$
$$\cdot ||\left(\Omega_A(f(H) - f(H'))\right)||$$
$$\cdot ||(I - \chi\Omega_A f(H'))^{-1}|| \qquad (42)$$

We can now use the inequality $||(I - A)^{-1}|| \leq 1/(1 - ||A||)$. It follows that

$$||(I - \chi\Omega_A f(H'))^{-1}|| \leq \frac{1}{1 - \chi||\Omega_A f(H)||}, \qquad (43)$$

where $||\Omega_A f(H)|| = \overline{\sigma}(\Omega_A f(H))$ is the minimum eigenvalue of $\Omega_A f(H)$, which is a semi-positive matrix with maximum eigenvalue 1. This implies that, and thus the matrix is upper bounded by $1/(1 - \chi)$. We thus have

$$||\vec{y}_{k+1}||_2 \leq (1-\alpha')||\vec{y}_k||_2 + \frac{\chi||\vec{M}||_2}{(1-\chi)^2\beta'}||\Omega_A(f(H)-f(H'))||. \qquad (44)$$

We note that $f : [0, 1] \to [0, 1]$, and that $f(H)$ is a diagonal matrix. It follows that if we introduce $||\Omega_A(f(H)-f(H'))|| = ||\vec{f}(H) - \vec{f}(H')||_2 \leq C_1||\vec{y}_k||_2$, we have

$$||\vec{y}_{k+1}||_2 \leq (1 + \alpha')||\vec{y}_k||_2 + C_1\frac{\chi||\vec{S}||_2}{(1-\chi)^2\beta'}||\vec{y}_k||_2$$
$$= \left(1 - \alpha' + \frac{C_1\chi}{(1-\chi)^2}\frac{||\vec{S}||_2}{\beta'}\right)||\vec{y}_{k+1}||_2 \qquad (45)$$

We thus find that if

$$C_1\frac{\chi||\vec{S}||_2}{(1-\chi)^2\beta'} < \alpha' \qquad (46)$$

then we have the contracting property. Rewritten, we have the following inequality:

$$||\vec{S}||_2 < \frac{(1-\chi)^2\alpha\beta}{\chi C_1} \qquad (47)$$

from which get that as long at the system is input-led with small enough voltages or currents, a memristor network satisfies the contracting property which is independent from the time step, as one would expect. If we read-out the resistive states, then the proof ends here, as the resistive states are continuous functions of the internal states. If instead we read out the voltage across the motif, then we need to show that this implies that also the voltage states are the same.

We now have two possibilities. If we input the system with voltage in series with the resistor (or memristor), then this implies that the voltage on the j-th motif is $V_{ro}^j(t) = V_c^j(t) + i_j(t)R_j(\eta(t))$, where V_{ro}^j is the read-out function. In this case, as long as the current is non-zero almost everywhere, then the echo state property is valid. In the case in which the current source is in parallel to the motif, then we have a voltage input function of the form $V_c^j(I_c(t))$ which is not easily related to the voltage source, but the argument is equally valid.

State Separability

As a measure of state separability, we ask that $||\vec{\eta}_{k+1} - \vec{\eta}'_{k+1}||_2 \geq 0 \,\forall t$. For the case memristor reservoirs we consider two identical initial states $\vec{x}_0$, but with different input (driving), $\vec{S}_1$ and $\vec{S}_2$. We would like to prove that the time evolution of

the two states is such that $||\vec{y}_k||_2$ diverges, e.g. it is always greater than zero.

We have

$$||\vec{y}_{k+1}||_2 = ||\vec{\eta}_{k+1} - \vec{\eta}'_{k+1}||_2$$

$$= ||(-\frac{1}{\beta}(1 - \chi\Omega f(H_k))^{-1}(\vec{S}_1 - \vec{S}_2)||_2 \quad (48)$$

Now, since the matrix

$$\frac{1}{\beta}(I - \chi\Omega f(H_k))^{-1}$$

has a trivial kernel for arbitrary $f(H_k)$, this is sufficient to show that if $\vec{S}_1 - \vec{S}_2 \neq 0$, then necessarily

$$||\vec{y}_{k+1}||_2 > 0 \; \forall \vec{x}_k. \quad (49)$$

This is sufficient to show that the trajectories must be locally diverging, and that thus the reservoirs have different internal states. This is a local version of the state separability as it is a local (in time) rather than global condition, but if we can show that already at this level not all input allow the states to diverge, then this cannot hold at a global level.

Now, if the voltage or the current sources are at the nodes, it is true that for sufficiently small (different) inputs $\vec{S}_{ext}$ and $\vec{j}_{ext}$ the state separability cannot be always preserved. This is due to the fact that the operators $A(A^T A)^{-1}$ and $B^T(BB^T)^{-1}$ can have non-trivial kernels. The reason can be easily seen if the memristor network is input-led via voltage sources in series or currents in parallels, there can be redundancy in the input. In fact, if

$$\vec{j}^1_{ext} = \vec{j}^2_{ext} + (I - \Omega_B)\vec{k}$$
$$\vec{S}^1_{ext} = \vec{S}^2_{ext} + (I - \Omega_A)\vec{k} \quad (50)$$

for arbitrary $\vec{k}$, we will have $\vec{S}_1 - \vec{S}_2 = 0$ identically. We can thus construct simple counterexamples for which the state evolution is identical for completely different inputs, and violates the state separability property. This is due to a freedom in defining the voltage drops on the edge, and is reflected in how we can input the system. This property has been described in previous papers. Thus, state separability is true as long as different inputs are not equal up to the transformation described in eqn. (50).

Solution of LRC circuits

An LRC circuit has the long time limit solution,

$$\begin{bmatrix} q(t) \\ \dot{q}(t) \end{bmatrix} = \frac{1}{l(\lambda_+ - \lambda_-)}\begin{bmatrix} 1 & 1 \\ \lambda_+ & \lambda_- \end{bmatrix}\begin{bmatrix} \int_0^\infty d\tau\, e^{\lambda_+ \tau}u(t-\tau) \\ -\int_0^\infty d\tau\, e^{\lambda_- \tau}u(t-\tau) \end{bmatrix} \quad (51)$$

where $\lambda_\pm = -\frac{r}{2l} \pm i\sqrt{\frac{1}{lc} - \frac{r^2}{4l^2}} = -\gamma \pm i\omega$.

Given a γ and $\Delta\omega$, we choose $l_n = 1$, $r_n = 2\gamma$ and

$$c_n = \frac{1}{n^2\Delta\omega^2 + \gamma^2} \quad (52)$$

in which case we have that the resulting LRC circuits have eigenvalues $\lambda_{n,\pm} = -\gamma \pm in\Delta\omega$. The resulting trajectories of the system are

$$q_n(t) = \frac{1}{ln\Delta\omega}\int_0^\infty d\tau\, e^{-\gamma\tau}\sin(n\Delta\omega\tau)u(t-\tau)$$

$$\dot{q}_n(t) = \frac{1}{ln\Delta\omega}\int_0^\infty d\tau\, e^{-\gamma\tau}[n\Delta\omega\cos(n\Delta\omega\tau)-$$
$$\gamma\sin(n\Delta\omega\tau)]\,u(t-\tau). \quad (53)$$

As noted in the main text, a linear transformation of these trajectories can be expressed in a form that resemble the familiar Fourier transform.

$$x_n(t) = \int_0^\infty d\tau\, e^{-\gamma\tau}\sin(n\Delta\omega\tau)u(t-\tau) \quad (54)$$

$$y_n(t) = \int_0^\infty d\tau\, e^{-\gamma\tau}\cos(n\Delta\omega\tau)u(t-\tau). \quad (55)$$

The set of frequencies ranging from $\Delta\omega$ to $N\Delta\omega$ set the bandwidth of signals that the network can reconstruct, while γ imposes a cutoff time. In order for the network to perform reconstructions, this should suppress the input outside of an interval given by the lowest frequency $\Delta\omega \sim \frac{1}{\tau}$. We thus choose $\gamma = \tau$ in our construction of LRC networks.

Volterra Series Solution of Memristor Equations

For a single memristor we can use the expansion of the inverse and integrate out the linear term to write the equation as

$$\frac{d}{dt}(e^{\alpha t}x) = \frac{1}{\beta}e^{\alpha t}\sum_{n=0}^\infty (\chi x)^n u(t). \quad (56)$$

Then integrating and taking the long time limit, we have a formal expression for x as,

$$x(t) = \frac{1}{\beta}\sum_{n=0}^\infty \chi^n \int_0^\infty d\tau\, e^{-\alpha\tau}x^n(t-\tau)u(t-\tau). \quad (57)$$

We assume a solution in the form of a Volterra series expansion,

$$x(t) = h_0 + \int_0^\infty d\tau_1\, h_1(\tau_1)u(t-\tau_1)$$

$$+ \int_0^\infty d\tau_1 d\tau_2\, h_2(\tau_1,\tau_2)u(t-\tau_1)u(t-\tau_2) + \cdots \quad (58)$$

$$= h_0 + \sum_{n=0}^\infty H_n u. \quad (59)$$

Inserting this into eqn. (57) and matching powers of u we have

$$h_0 = 0 \quad (60)$$

$$H_1 u = \frac{1}{\beta}\int_0^\infty d\tau_1 e^{-\alpha\tau_1}u(t-\tau_1) \quad (61)$$

$$H_2 u = \frac{\chi}{\beta^2}\int_0^\infty d\tau_1 \int_{\tau_1}^\infty d\tau_2\, e^{-\alpha\tau_2}u(t-\tau_1)u(t-\tau_2) \quad (62)$$
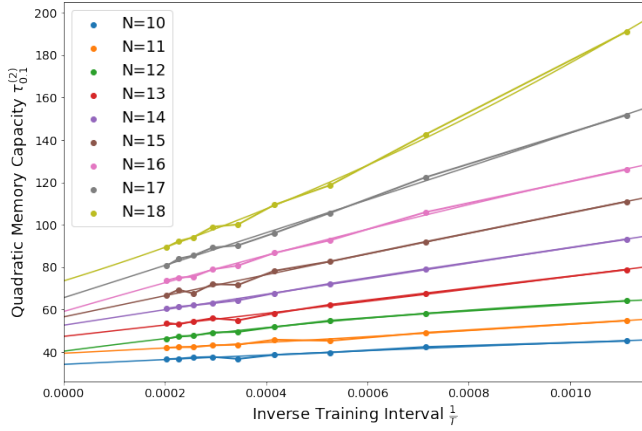
Figure 9. The finite size scaling analysis of quadratic memory capacities in hybrid LRC→Memristor reservoirs. Estimates from simulations are shown by circular makers connected by thick lines. Sizes in the legend are that of the surface LRC reservoir (number of subcircuits). A surface LRC reservoir of size N corresponds to $8N^2 - 2N$ total trajectories. Estimates of the quadratic memory capacity are shown as a function of the inverse training time $\frac{1}{T}$. A 2nd-order polynomial fit is also shown at each size. The capacities given in the main text correspond to the values of the fit at $\frac{1}{T} = 0$.

with subsequent powers following similarly. We immediately observe that: the nonlinear kernels produced by memristors are moderated by powers of $0 \leq \chi \leq 1$, and the kernels take the form of low pass filters of products of the input signal, decaying at a rate governed by α.

For the case of networks of memristor elements, the same manipulations lead to a formal expression for $x(t)$ which includes the effect of interactions through the cycle space projector Ω,

$$x(t) = \frac{1}{\beta} \sum_{n=0}^{\infty} \chi^n \int_0^\infty d\tau \, e^{-\alpha\tau} (\Omega X(t-\tau))^n \Omega \vec{u}(t-\tau). \quad (63)$$

This leads to corresponding terms in the expansion

$$h_0 = 0 \quad (64)$$

$$H_1 u = \frac{1}{\beta} \int_0^\infty d\tau_1 e^{-\alpha\tau_1} \Omega \vec{u}(t-\tau_1) \quad (65)$$

$$H_2 u = \frac{\chi}{\beta^2} \int_0^\infty d\tau_1 \int_{\tau_1}^\infty d\tau_2 \, e^{-\alpha\tau_2} \Omega U(t-\tau_1) \Omega u(t-\tau_2) \quad (66)$$

where we have used the convention $U = \mathrm{diag}(\vec{u})$.

Finite Size Scaling of Quadratic Memory Capacities

As noted in the main text, the quadratic memory capacities $\tau_\epsilon^{(2)}$ show a tendency towards overestimation for finite training intervals. This may be seen clearly in figure 9 where we have plotted the quadratic capacities for various reservoir sizes estimated from simulation against the inverse training time $\frac{1}{T}$. The sizes given in the figure legend correspond to the number of subcircuits in the surface LRC reservoir while the total number of trajectories in each reservoir is $8N^2 - 2N$. For each size, a 2nd-order polynomial fit is also plotted. Fits were performed using Numpy's polyfit function and the constant parameter was taken as the limiting value as $\frac{1}{T} \to 0$. These are plotted against reservoir size in the main text, figure 6.

[1] H. Jaeger, *The "echo state" approach to analysing and training recurrent neural networks-with an erratum note*, Tech. Rep. 148.34 (Bonn, Germany: German National Research Center for Information Technology GMD, 2001).

[2] H. Jaeger, in *GMD-German National Research Institute for Computer Science (2002), http://www.faculty.jacobs-university.de/hjaeger/pubs/STMEchoStatesTechRep.pdf* (Citeseer, 2002).

[3] M. Lukoševičius, in *Neural networks: Tricks of the trade* (Springer, 2012) pp. 659–686.

[4] N. Bertschinger and T. Natschläger, Neural computation **16**, 1413 (2004).

[5] H. Jaeger and H. Haas, science **304**, 78 (2004).

[6] J. Pathak, B. Hunt, M. Girvan, Z. Lu, and E. Ott, Physical review letters **120**, 024102 (2018).

[7] G. Tanaka, T. Yamane, J. B. Héroux, R. Nakane, N. Kanazawa, S. Takeda, H. Numata, D. Nakano, and A. Hirose, Neural Networks **115**, 100 (2019).

[8] L. Chua, IEEE Transactions on circuit theory **18**, 507 (1971).

[9] D. B. Strukov, G. S. Snider, D. R. Stewart, and R. S. Williams, Nature **453**, 80 (2008).

[10] A. Zegarac and F. Caravelli, EPL (Europhysics Letters) **125**, 10001 (2019).

[11] F. Caravelli and J. P. Carbajal, Technologies **6**, 118 (2018).

[12] L. Appeltant, M. C. Soriano, G. Van der Sande, J. Danckaert, S. Massar, J. Dambre, B. Schrauwen, C. R. Mirasso, and I. Fischer, Nature communications **2**, 1 (2011).

[13] J. Torrejon, M. Riou, F. A. Araujo, S. Tsunegi, G. Khalsa, D. Querlioz, P. Bortolotti, V. Cros, K. Yakushiji, A. Fukushima, *et al.*, Nature **547**, 428 (2017).

[14] M. J. Marinella and S. Agarwal, Nature Electronics **2**, 1 (2019).

[15] M. S. Kulkarni and C. Teuscher, in *2012 IEEE/ACM International Symposium on Nanoscale Architectures (NANOARCH)* (IEEE, 2012) pp. 226–232.

[16] C. Du, F. Cai, M. A. Zidan, W. Ma, S. H. Lee, and W. D. Lu, Nature communications **8**, 2204 (2017).

[17] J. P. Carbajal, J. Dambre, M. Hermans, and B. Schrauwen, Neural Computation **27** (2015), 10.1162/NECO_a_00694, arXiv:1406.2210.

[18] V. Athanasiou and Z. Kokoli, Sc. Rep. **10** (2020).

[19] W. Maass, T. Natschläger, and H. Markram, Neural computation **14**, 2531 (2002).

[20] W. Maass, P. Joshi, and E. D. Sontag, PLoS Comput Biol **3**, e165 (2007).

[21] J. Dambre, D. Verstraeten, B. Schrauwen, and S. Massar, Scientific reports **2**, 514 (2012).

[22] M. Hermans and B. Schrauwen, Neural Networks **23**, 341 (2010).

[23] M. Inubushi and K. Yoshimura, Scientific reports **7**, 10199 (2017).

[24] O. L. White, D. D. Lee, and H. Sompolinsky, Physical review letters **92**, 148102 (2004).

[25] F. Caravelli, F. L. Traversa, and M. Di Ventra, Physical Review E **95**, 022140 (2017).

[26] S. Boyd and L. Chua, IEEE Transactions on circuits and systems **32**, 1150 (1985).

[27] C. Gallicchio, A. Micheli, and L. Pedrelli, Neurocomputing **268**, 87 (2017).

[28] C. F. Sheldon and F. Caravelli, to appear **-**, (2020).